Can Tho University Journal of Science
website: sj.ctu.edu.vn

DOI: 10.22144/ctu.jen.2017.037

Molecular dynamics simulation of rutile - anatase heterojunction

Ca Nguyen Anh Khoa[1], Huynh Anh Huy[2]
[1]Hoang Thai Hieu High School, Vinh Long, Vietnam
[2]School of Education, Can Tho University, Vietnam

Article info.

Received 08 Jul 2016
Revised 12 Sep 2016
Accepted 29 Jul 2017

Keywords

DFTB method, molecular dynamics simulation, mixed phase, photocatalysis, rutile-anatase heterojunction

ABSTRACT

Density functional based tight-binding (DFTB) method was used to study the structural properties and electronic structure of heterojunction between anatase (100) and rutile (100) surface. The near coincidence site lattice (NCSL) theory was used to construct initial models. The interfaces have been annealed from 0K to 2250K in the linear ramp of 10 ps, followed by equilibration at the constant temperature of 2250 for 5 ps and cooled down 0K with an exponential ramp of 15 ps. Interface structures have been investigated via the partial radial distribution functions (PRDF), coordination number, bond-angle distributions and interatomic distances. The findings showed that both structures have the slightly disorder at the interfaces and the presence of four-coordinate Ti atoms, band offsets are 0.45 eV in the conduction band (CB) while 0.51 eV in the valence band (VB) with rutile is higher than anatase. Electrons migrate from rutile to anatase, while holes migrate in the opposite direction.

Cited as: Khoa, C.N.A., Huy, H.A., 2017. Molecular dynamics simulation of rutile - anatase heterojunction. Can Tho University Journal of Science. Vol 6: 140-147.

1 INTRODUCTION

In the past three decades, titanium dioxide (TiO_2) has been widely studied as one of the most promising semiconductor photocatalysts for its various applications in photocatalysis and photoelectrochemistry due to its superior photocatalytic activity, chemical stability, low cost, and nontoxicity (Ming, 2014). However, its wide band gap (3.2 eV for anatase and 3.0 eV for rutile) (Serpone, 2006) only allows TiO_2 to be excited by UV light (accounting for merely 4-5% sun light spectrum). This is the major constraint for the practical application of TiO_2 photocatalyst. Besides, the recombination between electron-hole can also reduce photocatalytic efficiency. Extensive research has been carried out to prepare TiO_2 photocatalyst such as doping of TiO_2 with various transition metal ions (Fe, Co, Ag, Ni) (Xin *et al.*, 2005; Choi *et al.*, 2010; Carneiro *et al.*, 2014) and non-metal (C, N, F, S) (Umebayashi *et al.*, 2003; Park *et al.*, 2009; Pelaez *et al.*, 2009). Nevertheless, most of the current methods of synthesizing doped TiO_2 nanoparticles face some issues like low production yield and use of some toxic chemical compounds. In addition, another method can also increase photocatalytic efficiency by using mixed phase anatase-rutile. The reason for the increment is, however, still under debate, but could involve several factors, i.e. bulk charge separation, special interfacial reaction sites like low coordinated Ti. The potential barrier at the interface was proposed to explain this increment. Actually, mixing two materials which have different band gap energies will create a potential barrier. Electrons and holes photo-generated transferred in the opposite direction each other across the interface decrease the recombination between them.

Over the years, mixed phase anatase-rutile has been intensively investigated by both experiment and computer simulation. Using X-ray photoelec-

tron spectroscopy, Bickley *et al*. (1991) concluded that the conduction band edge of rutile is lower than that of anatase. In contrast, the valence band edge of rutile is higher than that of anatase, and the holes from anatase pass through the rutile. In another study, based on electron paramagnetic resonance (EPR) measurement, Scotti *et al.* (2008) found that holes and electron were preferentially trapped on O^- and Ti^{3+} centers of the rutile phase, even when anatase is the main component. This indicates that electron transfer occurs from the higher energy conduction band states of anatase to those of rutile at lower energy, simultaneously, hole transfer occurs from the lower energy valence band states of anatase to those of rutile at higher energy.

Recently, Deák *et al.* (2011) have calculated the branching point energy (or charge neutrality level) and shown that both conduction and valence band of rutile are higher ~0.35 eV and ~0.55 eV than anatase, respectively. This staggered alignment of the bands means that migrating holes accumulate in rutile, while electrons accumulate in anatase.

There are several conflicting reports on the direction of charge transfer while knowledge of the relative position of the conduction and valence band edges is the key to understand charge transfer process. Besides, there is no investigation describing in detail the structure of the interface between anatase and rutile, it is motivated to carry out the molecular dynamics (MD) simulation of rutile - anatase heterojunction.

2 METHODOLOGY

The derivation of Density Functional based Tight-Binding (DFTB) from DFT has been represented several times, for completeness, the equations were derived briefly; the emphasis is on the final expressions. As an approximation of DFT, DFTB is also formulated around an expression of the total energy *E* of the atomic system as a functional of the spatial distribution of electron density $n(\vec{r})$: $E=E\left[n(\vec{r})\right]$. The electron density in DFTB is expanded in a reference density plus a small fluctuation: $n(\vec{r})=n_0(\vec{r})+\delta n(\vec{r})$. For brevity, the notation $\int d^3\vec{r}\to\int$, $\int d^3\vec{r}'\to\int'$, $n(\vec{r})\to \mathrm{n}$, $n(\vec{r}')\to \mathrm{n}'$ was used, the total energy can be written as follows:

$$E[n]=\sum_i\langle\psi_i|-\frac{1}{2}\nabla^2+V_{ext}+\frac{1}{2}\int\frac{n_0'}{|\vec{r}'-\vec{r}|}d\vec{r}'+V_{xc}[n_0]|\psi_i\rangle + \frac{1}{2}\int\int'\left(\frac{1}{|\vec{r}'-\vec{r}|}+\frac{\delta^2E_{xc}}{\delta n\delta n'}\right)\delta n\delta n'+E_{\alpha\beta} + E_{xc}[n_0]-\int V_{xc}[n_0]n_0-\frac{1}{2}\int\int'\frac{n_0n_0'}{|\vec{r}'-\vec{r}|} \quad (1)$$

The first term in Eq. (1) is the band structure energy

$$E_{BS}=\sum_i^{occ}\langle\psi_i|\hat{H}^0|\psi_i\rangle$$

Where the Hamiltonian $\hat{H}^0$ itself contains no charge transfer.

The second term in Eq. (1) is the second-order correction E_{2nd}. In DFTB, the density fluctuations $\delta\rho(\vec{r})$ are approximated as charge fluctuations Δq_α on atom α

$$\Delta q_\alpha=q_\alpha-q_\alpha^0$$

Where q_α^0 is the number of valence electrons for a neutral atom,

$q_\alpha=\frac{1}{2}\sum_{\mu,\nu}\left(C_\mu^*C_\nu-C_\nu^*C_\mu\right)S_{\mu\nu}$ is the Mulliken population on atom α

Neglecting the term $\delta^2E_{xc}/\delta n\delta n'$ for the moment, the second-order term finally reads

$$E_{2nd}=\frac{1}{2}\sum_{\alpha,\beta}\gamma_{\alpha\beta}\Delta q_\alpha\Delta q_\beta$$

The last four terms in Eq. (1) are collectively called the repulsive energy because of the ion-ion repulsion term, but it contains also xc-interactions, so it is a complicated object. In DFTB, this term is approximated by a sum of pair potentials called repulsive energy term

$$E_{rep}=\sum_{\alpha\neq\beta}V_{\alpha\beta}^{rep}\left[\vec{R}_{\alpha\beta}\right]$$

This term is either determined by comparison with DFT calculations or fitted to empirical data. The total energy, then, reads

$$E[n]=E_{BS}+\frac{1}{2}\sum_{\alpha,\beta}\gamma_{\alpha\beta}\Delta q_\alpha \Delta q_\beta+E_{rep} \quad (2)$$

The one-electron eigenstates ψ_i of the system are expanded in a linear combination of atomic orbitals (LCAO) $\{\varphi_\upsilon\}$ centered on the atomic sites $\vec{R}_A$

$$\psi_i=\sum C_{\mu i}\varphi_\mu(\vec{r}-\vec{R}_\alpha), \quad (3)$$

$c_{\nu i}$ being the variational coefficients minimizes the energy. The LCAO expansion transforms (2) in an algebraic system for the variational coefficients

$$\sum_\nu C_{\nu i}(H_{\mu\nu}-\varepsilon_i S_{\mu\nu})=0 \quad (4)$$

where $H_{\mu\upsilon}=H^0_{\mu\upsilon}+\frac{1}{2}S_{\mu\upsilon}\sum_{\alpha,\beta}\left(\gamma_{\alpha\zeta}+\gamma_{\beta\zeta}\right)\Delta q_\zeta$

and

$$H^0_{\mu\upsilon}=\left\langle\varphi_\mu\middle|\hat{H}_0\middle|\varphi_\mu\right\rangle=\begin{cases}\varepsilon_\mu^{neutral\ free\ atom} & for\ \mu=\upsilon\in A\\ \left\langle\varphi_\mu^\alpha\middle|\hat{H}_0\middle|\varphi_\mu^\beta\right\rangle & \alpha\neq\beta\\ 0 & otherwise\end{cases}, \quad (5)$$

$S_{\mu\nu}=\left\langle\varphi_\mu\middle|\varphi_\nu\right\rangle$ is the overlap matrix. The Hamilton matrix elements depend on the Mulliken charges q_α which in turn depend on the molecular orbital coefficients $C_{\nu i}$, thus these equations have to be solved self-consistently.

3 CALCULATION DETAILS

3.1 Building the anatase-rutile interface

Firstly, the surface of each phase was chosen to create the interface which is the most stable. The stability of the interface can be expressed by the adhesion energy E_{adh}, which is defined as the energy needed (per unit area) to reversibly separate the two phases. Recently, Deskins *et al.* (2007) have performed classical force field calculation for many interfaces. The interface between rutile (100) and anatase (100) was found to have the highest adhesion energy. Therefore, this interface was focusedly investigated in this work.

In order to construct initial models, the near coincidence site lattice (NCSL) theory was used to provide a framework to create surface interfaces for structures with incommensurate lattice parameters. This theory was described for the first times by Sayle *et al.* (1997) as applied to cubic and hexagonal systems. Fisher and Matsubara (2005) later extended the theory to rectangular systems. In NCSL theory, the interface between anatase (100) and rutile (100) surface can be considered as 2D rectangular lattice. The area A of the interface is chosen to keep the conservation of periodicity of both phases. Hence, the length and width of simulation box are the least common multiples of the length and width of unit cells in both phases, i.e. these rectangular edges must satisfy the relationship

$$\begin{aligned} n_1 a_a &= n_2 a_r \\ m_1 c_a &= m_2 c_r \end{aligned}.$$

Where n_1, n_2, m_1, m_2 are integer and adjustable; a_a = 3.8908Å, c_a = 9.3671Å, a_r = 4.6717Å, c_r = 2.9973Å are lattice constants of anatase and rutile, respectively, obtained by optimization primitive cells of these phases, using DFTB+ code.

The misfit percentage values along the length and width of the interface are defined as

$$M_m=\left(1-\frac{m_1 c_a}{m_2 c_r}\right)100 \quad \text{and} \quad M_n=\left(1-\frac{n_1 a_a}{n_2 a_r}\right)100.$$

To produce the interface with minimal misfit, the rutile slab needs rotating 90^0 relative to the other around an axis perpendicular to the interface, so a_r and c_r are switched in relationships above. Furthermore, the misfit can be also decreased by deformation (shrinking or stretching) one or both lattices by adjust their lattice constants. According to the analysis above, it determined n_1=3, n_2=4, m_1=1, m_2=2 and lattice constants are shown in table 1 (i.e. the interface have 3 anatase and 8 rutile unit cells with the misfit M_n = 2.64%, M_m = –0.25%). The formation of interface between anatase (100) and rutile (100) surfaces according to NCSL theory is presented in Figure 1.

Table 1: The lattice parameters of anatase and rutile from Experiment, DFTB, NCSL theory and the misfit of NCSL theory respect to DFTB

		Experiment	DFTB	NCSL Theory	Misfit (%)
Anatase	a(Å)	3.782	3.8908	3.95628	1.68
	c(Å)	9.502	9.3671	9.35562	0.12
Rutile	a(Å)	4.587	4.6717	4.67781	0.13
	c(Å)	2.954	2.9973	2.96721	1.00

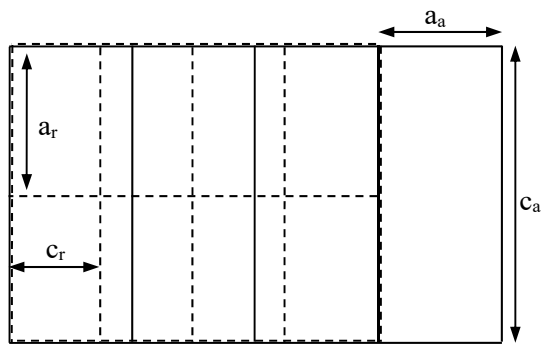

Fig. 1: Formation of interface between anatase (100) and rutile (100) surfaces according to NCSL theory. In this case, we have 3aa = 4cr and 1ca = 2ar

From the data above, one anatase and one rutile slab were cut, then, aligned to create the interface in monolayer model having a simulation box size of 52.40Å×9.36Å×11.87Å (consists of 372 atoms). It is noted that a vacuum layer of 15Å thickness was added to the simulation box of monolayer model to conservation of periodicity in three dimensions. Similarly, two anatase slabs and one rutile slab were cut, then, aligned to create the interface in multilayer model having the simulation box size of 43.08Å×9.36Å×11.87Å (consists of 408 atoms). The initial interfaces in monolayer and multilayer model are shown in Figures 2 and 3.

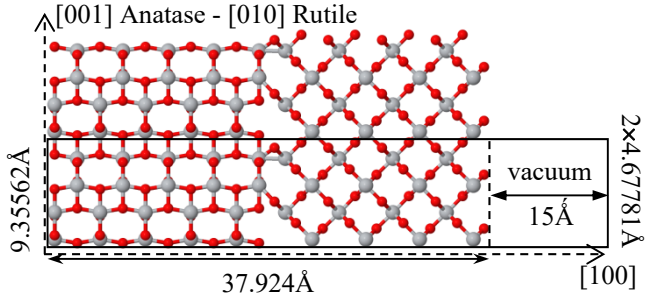

Fig. 2: Initial monolayer model and its simulation box

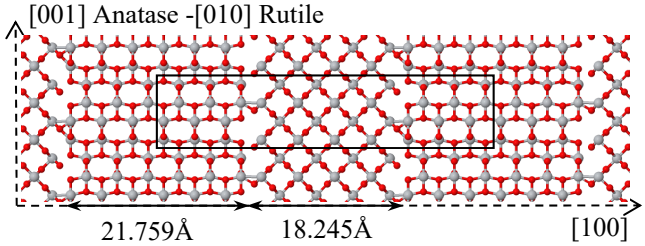

Fig. 3: Initial multilayer model and its simulation box

3.2 MD simulation

In order to obtain plausible models of the rutile-anatase interface, rutile and anatase slabs were "welded" by simulated annealing these models reaching in melting temperature of two phases. This step allows the slabs to achieve such bonding and adhesion each other. After that, these models were cooled down 0K to comeback solid state.

Molecular dynamic calculations were carried out by using the Self Consistent Charge Density Functional Tight Binding scheme (SCC-DFTB) and using the DFTB+ code, this is the free code for uncommercial purposes, it can be downloaded at http://www.dftb-plus.info. The temperature of the models was increased linearly to 2250K in time as $T(t) = T_0 + \gamma t$; here γ is an annealing rate of 2.25×10^{14} Ks^{-1}, and T_0 is the initial temperature of 0K. After reaching 2250K, these models were followed by equilibration at the constant temperature of 2250 for 5 ps, and an exponential cooling curve down to 0K for 15ps. Finally, these models were relaxed at 0K until their energies are minimum.

Interface structures were investigated via the partial radial distribution functions (PRDF), coordination number, bond-angle distributions and interatomic distances. In order to calculate the coordination number and bond-angle distributions, $R_{Ti\text{-}O}$ = 2.35 Å, $R_{Ti\text{-}Ti}$ = 3.35 Å, $R_{O\text{-}O}$ = 3.15Å were adopted. Here R denotes a cutoff radius, which is chosen as the position of the minimum after the first peak in the PRDF. Electronic structure of the interfaces

was investigated via band offset in the CB and VB and density of state.

4 RESULTS AND DISCUSSION

4.1 Interface structure

In this work, the structure of three different interfaces including one in monolayer model (denoted as interface 1) and two in multilayer model (denoted as interface 2 and interface 3) was studied. The 3D pictures of interfaces formed by anatase (100) and rutile (100) surfaces in monolayer and multilayer models are shown in Figures 4 and 5. These pictures suggested that there is some disorder at the interfaces with the transition of Oxygen from anatase to rutile because rutile is more stable. In addition, the existence of four-coordinated Ti interfacial atoms (Ti_{4C}) was recognized, while in the initial interfaces Ti atoms only have coordinated 5 (Ti_{5C}) or 6 (Ti_{6C}). The binding between anatse and rutile slabs is mainly created by tetrahedral structures (TiO_4). These results are similar to the investigation of Tanaka *et al.* 2002 based on UV/Vis diffuse reflectance and X-ray absorption fine structure (XAFS) measurments. Additionally, the study of Hurum *et al*. (2006) suggested that the occurrence of Ti_{4C} contributed to reducing the recombination of electrons-holes and increasing photocatalytic efficiency.

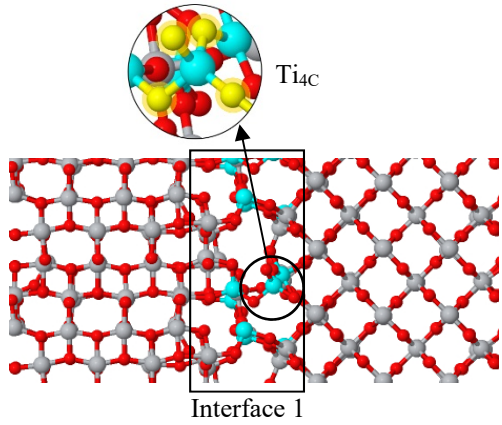

Fig. 4: Final monolayer model and Ti_{4C} (small picture). Cyan and yellow circles indicate the Ti_{4C} atoms and O around them, respectively

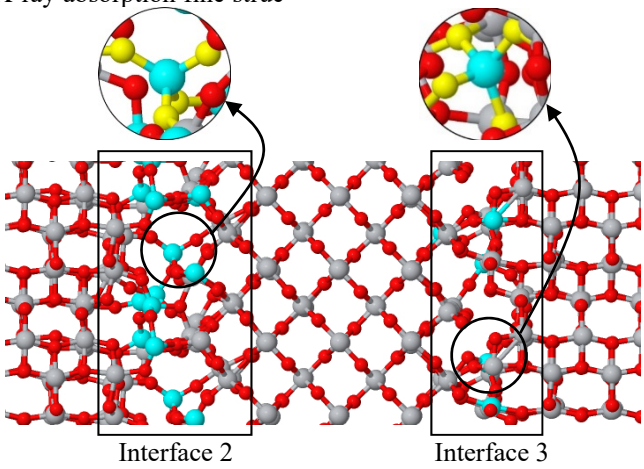

Fig. 5: Final multilayer model and and Ti_{4C} (small picture). Cyan and yellow sphere indicate the Ti_{4C} atoms and O around them, respectively

To provide insight into the interface structure beside 3D pictures, the PRDF for Ti-O pairs at the interface was firstly examined and compared with the bulk model (Petkov *et al.*, 1998). In the graphs of PRDF of anatase and rutile bulks (Figure 6a and 6b) distinct peaks indicate high crystallinity, but at the interfaces (Figures 6c and 6e), the first peak is lower, and the others become less distinct. Moreover, the RDF drops to zero between the neighbor peaks in the bulks, whereas at the interfaces, this is not the case. Therefore, it can be concluded that the structure of interfaces is amorphous. However, there is no data about the interface structure between anatase and rutile being found. Hence, the structural parameters calculated are compared with the results of Petkov *et al.* (1998). The interatomic distances details between Ti-O, Ti-Ti and O-O of all interfaces are shown in Table 2. The Ti-O bond length of interfaces varies between 1.90 Å and 1.92 Å, this length is shorter than the one in amorphous TiO_s nanoparticles like those observed in experiment for the bulk (Petkov *et al.*, 1998).

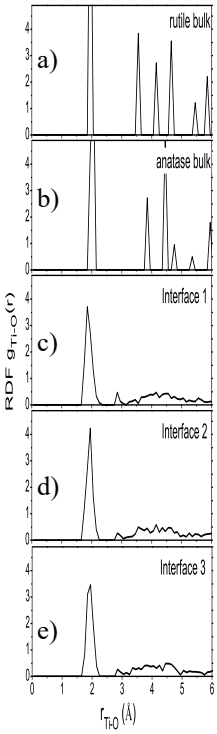

Fig. 6: Radial distribution Functions for Ti-O pair at the interfaces compared to anatase and rutile bulks

In the graph of PRDF for Ti-Ti pair, it can be seen the splitting of the first peak at interface 2 and interface 3. This means that both linking of octahedral by the edge and vertex occur in these interfaces. Here, the first peak is centered at around 3.05 Å represent the linking between two structural units sharing an edge, and the second one is at 3.45 Å represent the linking between two structural units have a common vertex. These values are very close to 3.00 Å and 3.55 Å obtained in experiment, respectively. On the other hand, no splitting at interface 1 was found because of non-existence of Ti_{6c} in this interface.

More details about the structure of interfaces can be found via the coordination number distribution for Ti-O pair (Figure 7). This distribution also indicated the existence of Ti_{4C} atoms. In all three interfaces, the fraction of Ti_{6C} was decreased, while the number of Ti_{5C} was virtually negligible changed. Especially, there was no six-coordinated Ti interfacial atom was found at interface 1, i.e. during annealing and cooling process, the structural units transformed from octahedral to tetrahedral structure.

Table 2: The details of interatomic distances between Ti-O, Ti-Ti and O-O at the interfaces and comparison to bulk amorphous

Materials	r (Å)		
	Ti-O	O-O	Ti-Ti
Interface 1	1.90	2.94	3.10
Interface 2	1.92	2.93	3.05-3.45
Interface 3	1.92	2.91	3.05-3.45
Exp. For bulk amorphous	1.96	2.67	3.00-3.55

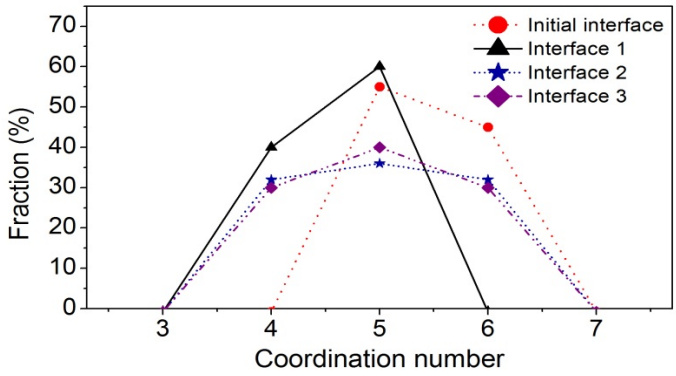

Fig. 7: Coordination number distributions at the interfaces before and after simulation process

4.2 Electronic structure

One another reason for the increment of photocatalytic efficiency of mixed phase anatase-rutile is charge transfer direction across the interface, which depends on the alignment of the CB minimum and VB maximum between anatase and rutile.

Theoretical work generally indicates that photogenerated electrons may migrate from rutile to anatase, while holes may migrate to the rutile phase. Using the technique by Walle, Kullgren calculated the jumps of an average electrostatic potential across the interface, and indicated that the VB offset and CB offset were 0.86eV-0.65eV at the rutile (100)-anatase (100) and 0.90eV-0.69eV at the rutile (110)-anatase (101) with rutile is higher in the both bands (Kang *et al*., 2012).

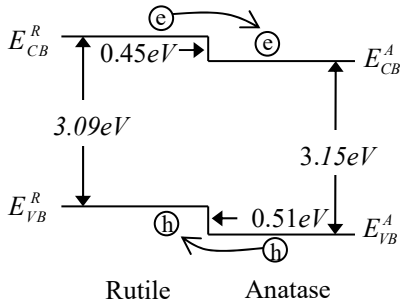

Fig. 8: Schematic representation of the band line-up between anatase and rutile

The key to align energy levels of two materials is to find a common reference level such as vacuum level or some other common level. Using the branching point energy (Deák *et al*., 2011), it found that the band lineups between anatase-rutile is 0.45 eV in the CB and 0.51 eV in the VB higher than anatase ones. Schematic representation of the band line-up between anatase and rutile is shown in Figure 8. This staggered alignment of the band means that electrons move from rutile to anatase, while holes move in the opposite direction.

In order to further examine the effect of interface, an analysis of the density of state (DOS) of anatase and rutile was performed (Figure 9). The result from DOS also agrees with the previous offset result in that the bulk CB and VB rutile are both higher than of anatase. Additionally, in this calculation it was also found that the band gaps of anatase and rutile are 3.15 eV and 3.09 eV. These values are in excellent agreement with the result of Tang *et al.* (1993). Whereas, the interfaces have smaller band gaps (2.12 eV). This decrease due to the contribution of Oxygen *2p* at the valence band of rutile and Titanium *3d* at the conduction band of anatase (Figures 10 and 11).

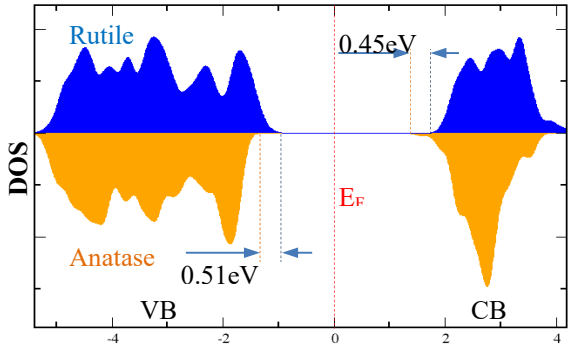

Fig. 9: Comparison of the DOS of rutile and anatase. The energy scales have been aligned based on the bottom of valence band

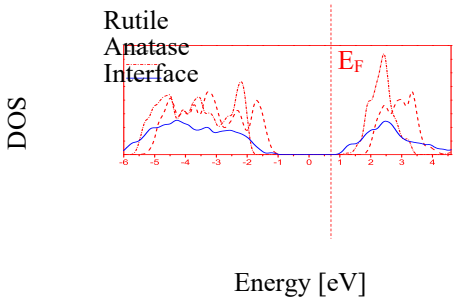

Fig. 10: Density of State of anatase, rutile bulk and interface

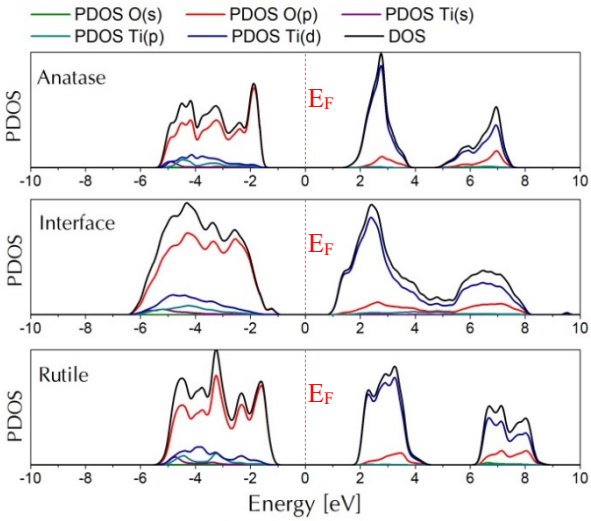

Fig. 11: Projected Density of State of anatase, rutile bulk and interface

5 CONCLUSIONS

In the research, the interfaces were created in two models, monolayer and multilayer model. The structural properties of the interfaces were described in detail via 3D pictures, RDF, interatomic distances and coordination number distributions. It indicated that interfaces had amorphous structure.

At two interfaces in multilayer model existed both linking of octahedral by the edge and vertex that was represented by the splitting at the first peak in PRDF for Ti-Ti pair, but this was not happen at the interface in monolayer model.

The presence of 4-fold coordinated Ti interfacial atoms at the interfaces was found to be one of the factors that increase the photocatalytic efficiency of mixed phase anatase-rutile by reducing the recombination of electrons-holes photo-generated.

Beside the determination of structural properties of models, their electronic structure was also studied. As calculated, the band offsets are 0.45 eV in the conduction band (CB) and 0.51 eV in the valence band (VB) with rutile ones are higher than anatase ones, so electrons photo-generated migrate from rutile to anatase, while holes migrate in the opposite direction. This phenomenon contributed to reduce the recombination between electrons and holes photo-generated, therefore, the photocatalytic efficiency of mixed phase anatase-rutile was increased.

REFERENCES

Bickley, R.I., Gonzalez-Carreno, T., Lees, J.S., Palmisanod, L., Tilley, R.J.D., 1991. A structural investigation of Titanium Dioxide photocatalysts. Journal of Solid State Chemistry. 92(1): 178-190.

Carneiro, J.O., Azevedo, S., Fernandes, F., Freitas, E., Pereira, M., Tavares, C.J., Lanceros-Mendéz, S., Teixeira, V., 2014. Synthesis of iron-doped TiO2 nanoparticles by ball-milling process: the influence of process parameters on the structural, optical, magnetic, and photocatalytic properties. Journal of Materials Science. 49: 7476-7488.

Choi, J., Park, H., Hoffmann, M.R., 2009. Effects of single metal-ion doping on the visible-light photoreactivity of TiO_2. The Journal of Physical Chemistry C. 114: 783-792.

Deák, P., Aradi, B., Frauenheim, T., 2011. Band lineup and charge carrier separation in mixed rutile-anatase systems. The Journal of Physical Chemistry C. 115(8): 3443-3446.

Deskins, N.A., Kerisit, S., Rosso, K.M., Dupuis, M., 2007. Molecular dynamics characterization of rutile-anatase interfaces. The Journal of Physical Chemistry C. 111: 9290-9298.

Fisher, C.A.J., Matsubara, H., 2005. Molecular dynamics simulation of interfaces between NiO and cubic ZrO2. Philosophical Magazine. 85: 1067-1088.

Hurum, D.C., Agrios, A.G., Crist, S.E., Gray, K.A., Rajh, T., Thurnauer, M.C., 2006. Probing reaction mechanisms in mixed phase TiO2 by EPR. Journal of Electron Spectroscopy and Related Phenomena. 150: 155-163.

Kang, J., Wu, F., Li, S.S., Xia, J.B., Li, J., 2012. Calculating Band Alignment between Materials with Different Structures: The Case of Anatase and Rutile Titanium Dioxide. The Journal of Physical Chemistry C. 116: 20765-20768.

Kullgren, J., Huy, H.A., Aradi, B., Frauenheim, T., Deák, P., 2014. Theoretical study of charge separation at the rutile-anatase interface. Physics Status Solidi RRL 8. 6: 566-570.

Ming, G.J., Guangxu, S., Wang, J., Meng, Q., Liang, W., 2014, Origin of High Photocatalytic Properties in the Mixed-Phase TiO2: A First-Principles Theoretical Study, ACS Applied Materials & Interfaces. 6 (15): 12885-12892.

Park, Y., Kim, W., Park, H., Tachikawa, T., Majima, T., Choi, W., 2009 Carbon-doped TiO2 photocatalyst synthesized without using an external carbon precursor and the visible light activity. Applied Catalysis B: Enviromental. 91: 355-361.

Pelaez, M., de la Cruz, A. A., Stathatos, E., Falaras, P., Dionysiou, D.D., 2009. Visible light-activated NF-codoped TiO2 nanoparticles for the photocatalytic degradation of microcystin-LR in water, Catal. Today 144: 19-25.

Sayle, T.X.T., Catlow, C.R.A., Sayle, D.C., Parker, S.C., Harding, J.H., 1993. Computer simulation of thin film heteroepitaxial ceramic interfaces using a near-coincidence-site lattice theory. Philosophical Magazine A. 68: 565-573.

Scotti, R., Bellobono, I.R., Canevali, C., Cannas, C., Catti, M., D'Arienzo, M., Musinu, A., Polizzi, S., Sommariva, M., Testino, A., Morazzoni, F., 2008. Sol-Gel Pure and Mixed-Phase Titanium Dioxide for Photocatalytic Purposes: Relations between Phase Composition, Catalytic Activity, and Charge-Trapped Sites. Chemistry of Materials. 20: 4051-4061.

Serpone, N., 2006. Is the Band Gap of Pristine TiO2 Narrowed by Anion- and Cation-Doping of Titanium Dioxide in Second-Generation Photocatalysts?. The Journal of Physical Chemistry B. 110: 24287-24293.

Tanaka, T., Teramura, K., Yamamoto, T., Takenaka, S., Yoshida, S., Funabiki, T., 2002. TiO2/SiO2 photocatalysts at low levels of loading: preparation, structure and photocatalysis. Journal of Photochemistry and Photobiology A. 148: 277-281.

Tang, H., Prasad, K., Sanjinès, R., Schmid, P.E., Lévy, F., 1994. Electrical and optical properties of TiO2 anatase thin films. Journal of Applied Physics. 75: 2042-2047.

Umebayashi, T., Yamaki, T., Tanala, S., Asai, K., 2003. Visible Light-Induced Degradation of Methylene Blue on S-doped TiO2. Chemistry Letters. 32: 330-331.

Xin, B., Jing, L., Ren, Z., Wang, B., Fu, H., 2005. Effects of Simultaneously Doped and Deposited Ag on the Photocatalytic Activity and Surface States of TiO2. The Journal of Physical Chemistry B. 109: 2805-2809.